Molecular Dynamics Simulation of Brittle Fracture in Silicon

J. G. Swadener, M. I. Baskes, and M. Nastasi

Materials Science and Technology Division, Los Alamos National Laboratory, Los Alamos, New Mexico 87545

(Received 12 February 2002; published 6 August 2002)

Brittle fracture in silicon is simulated with molecular dynamics utilizing a modified embedded atom method potential. The simulations produce propagating crack speeds that are in agreement with previous experimental results over a large range of fracture energy. The dynamic fracture toughness is found to be equal to the energy consumed by creating surfaces and lattice defects in agreement with theoretical predictions. The dynamic fracture toughness is approximately 1/3 of the static strain energy release rate, which results in a limiting crack speed of 2/3 of the Rayleigh wave speed.

DOI: 10.1103/PhysRevLett.89.085503 PACS numbers: 62.20.Mk, 02.70.Ns, 46.50.+a

The fracture process involves converting potential energy from a strained body into surface energy, thermal energy, and the energy needed to create lattice defects. In dynamic fracture, energy is also initially converted into kinetic energy. A material converts the stored potential energy from a distance of perhaps 100 mm from the crack tip into other forms of energy within a small number of atoms at the speed of sound, the details of which are not well understood. The crack speeds reported in previous experimental studies in silicon [1,2] indicate that surface energy alone will not satisfy the energy balance. In this study, molecular dynamics (MD) is used to simulate brittle fracture in silicon and determine how energy is converted from potential energy (strain energy) into other forms.

Previous MD simulations of fracture in silicon [1,3–6] overestimate the experimental crack speeds by 25%–50% at low applied loads, and at higher loads, fail to show the increase of crack speed with load shown by experiments. The difficulty in the earlier MD studies appears to be the reapportionment of converted potential energy between lattice defect energy and kinetic energy. The best results previously obtained are from Bernstein and Hess [6] who used a semiempirical tight binding potential for a few unit cells surrounding the crack tip, which are coupled to an environment dependent interatomic potential in the remainder of the model. In their model, fracture initiated at approximately 85% of the experimental static fracture toughness (J_{1C}), reached a peak speed at a slightly higher load ($J_s = 1.5J_{1C}$, where J_s is the strain energy release rate) and then decreased. Their results disagree with experimental results [1] where the crack speed continues to increase to the maximum applied load, which was $J_s = 7J_{1C}$.

The potential derived using the modified embedded atom method (MEAM) [7], has been shown to account for directional bonding and give accurate physical properties for silicon [8]. Correct values for these properties are found to be important, because many features, such as cleavage planes and dislocation generation, depend on specific crystallographic orientations and resolved stresses in specific directions. Calculations using the MEAM potential that are presented below are the first to determine the energy consumed by the creation of lattice defects during dynamic fracture and to explain the limiting speed of cracks in silicon. Bernstein and Hess [6] proposed that potentials with a relatively low peak stress in the force-separation response for (111) planes should produce brittle fracture. The peak stress for the MEAM potential (30 GPa), which shows brittle fracture, is greater than the peak stress shown in [6] for the tight binding potential and the Stillinger-Weber (SW) potential, the latter of which exhibits ductile fracture. Therefore the peak stress is not the most important factor that leads to brittle fracture.

Fracture on (111) and (110) planes in silicon has been shown [9–11] to obey the Griffith criterion: $J_{1C} = 2\gamma_0$, where γ_0 is the surface energy. This indicates that purely brittle cleavage with no energy dissipation occurs on these low energy planes, which is verified by experimental observations of atomically smooth fracture surfaces [1,2]. For dynamic fracture, additional energy is typically expended to accelerate material ahead of the advancing crack tip. In most cases, the dynamic fracture toughness (J_d) can be related to the crack speed (v) as [12]

$$\frac{J_d}{J_s} = 1 - \frac{v}{c_R}, \tag{1}$$

where J_s is the static strain energy release rate and c_R is the Rayleigh wave speed in the direction of crack propagation. J_s is the reduction in potential energy (due to release of strain) in the body per unit area of new crack surface created ($J_s = dU/d\mathrm{A}$). J_d is the portion of converted potential energy that is used to create new surfaces and lattice defects. For fracture on the (111) and (110) planes in silicon, experiments have shown that $J_d = J_{1C}$ for values of J_s up to $2J_{1C}$ [1,2]. For larger values of J_s, the experiments reveal that $J_d > J_{1C}$, indicating that some dissipation occurs. For values of J_s much larger than J_{1C}, crack branching can occur resulting in two (or more) dynamically propagating crack tips that consume up to twice as much energy (or more) as a single crack tip.

For the strip specimen geometry (Fig. 1) that will be used herein, the energy release rate can be written in terms of the relative displacement of the top and bottom surfaces (V) as [13]

$$J_s = \frac{V^2 E^*}{2H}, \tag{2}$$

where H is the total height of the strip and E^* is an effective modulus derived from the anisotropic elastic constants as given by Hutchinson and Suo [13].

Since, as indicated by Eqs. (1) and (2), physical constants play a pivotal role in dynamic fracture, accurate molecular dynamic simulation of dynamic fracture requires the use of a potential (such as the MEAM potential) that gives values for surface energy and elastic constants in good agreement with experimental values. Three models were used to determine if the model height had an effect on the fracture results. The dimensions of the models were $450 \times 20 \times 112$ Å, $450 \times 15 \times 147$ Å, and $599 \times 15 \times 239$ Å in the x, y, and z directions, respectfully. The largest model contained 111 000 atoms, and the other two models contained 56 000 atoms each. Periodic boundary conditions were applied in the y direction. The models were oriented so that the crack would lie in the x-y plane and propagate in the x direction as shown in Fig. 1. The x, y, and z directions were aligned with the $[2\bar{1}\bar{1}]$, $[01\bar{1}]$, and $[111]$ crystallographic directions, respectively. The models contained starter cracks that were 60–90% of the model height in length and formed by the removal of one plane of atoms. The simulations showed that the crack tip was well defined as a 3 Å separation between atoms. Therefore a cutoff radius of 6 Å was used with the MEAM potential.

Load was applied by first straining the lattice in tension in the z direction accompanied by contraction in the x and y directions equal to 25% of the z-direction strain. Next, displacements in the z direction were applied to the upper and lower surfaces at the rate of 0.25 Å/ps for a period of 1 to 4 ps. A wide range of load was applied by varying the initial strain from 4 to 9% and applying additional displacements. By varying the length of the starter crack, the load was applied while the crack accelerated, but before the crack had propagated past the midpoint of the specimen. Finally, the upper and lower surfaces were held fixed to provide a constant energy release rate while the crack propagated in the central region of the model.

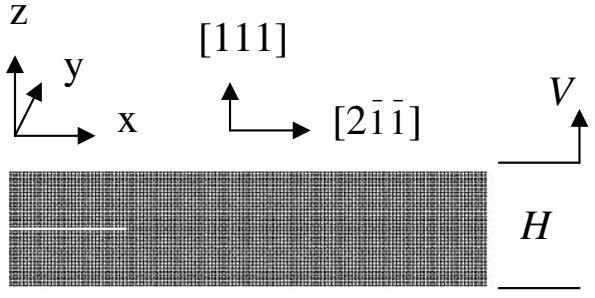

FIG. 1. Molecular dynamics model oriented with crystallographic axes as shown. Crack propagates in the $[2\bar{1}\bar{1}]$ direction.

Initially, atoms were given kinetic energy equivalent to a temperature of 300 K. In the upper third and lower third of each model, the temperature was maintained at approximately 300 K using a Nosé-Hoover thermostat [14,15] on only the velocities in the x and y directions. The temperature in the central third of the model was not controlled after the initial distribution of kinetic energy.

In order to simulate relatively large energy release rates, strains of up to 14% were applied to the models. At strains of that magnitude, the elastic constants of silicon are significantly reduced compared to the equilibrium condition. Therefore, in order to accurately calculate J_s in the MD simulations, the mean value of E^* was determined as a function of strain via

$$\frac{1}{2}\epsilon_{zz}^2 E^* = \frac{\Delta U}{\Omega}, \tag{3}$$

where ϵ_{zz} is the strain in the z direction, Ω is the atomic volume, and ΔU is the energy change for a homogenously strained sample ($\epsilon_{xx} = \epsilon_{yy} = -0.25\epsilon_{zz}$). The results for E^* are shown in Fig. 2, where the z direction is aligned with the [111] crystallographic direction. The variation of C_{33} with strain is also shown in Fig. 2 for comparison.

Because the elastic constants vary with strain, the Rayleigh wave speed also varies with strain. At zero strain, the MEAM potential gives $c_R = 4.71$ km/s for a Rayleigh wave traveling on a (111) surface in the $[2\bar{1}\bar{1}]$ direction. The comparable value calculated from the experimental elastic constants is $c_R = 4.68$ km/s. The Rayleigh wave speeds were determined from the anisotropic elastic constants using the method given by Darinskii [16]. For $\epsilon_{zz} = 0.14$ and $\epsilon_{xx} = \epsilon_{yy} = -0.035$, the relevant MEAM potential elastic constants are $C_{11} = 130.2$ GPa ($[2\bar{1}\bar{1}]$ direction), $C_{33} = 109.7$ GPa ($[111]$ direction),

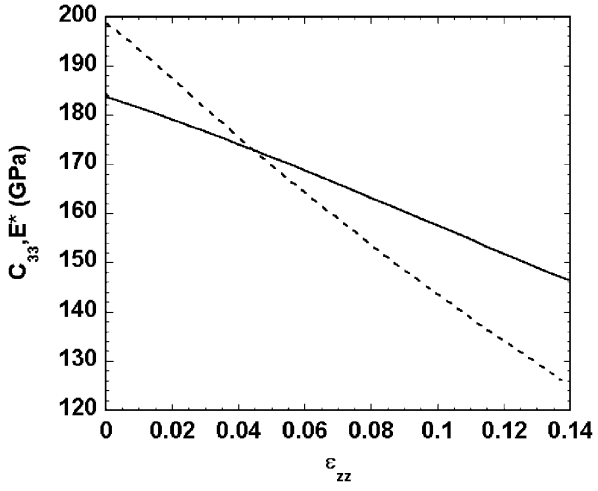

FIG. 2. Variation of C_{33} (for $\epsilon_{xx} = \epsilon_{yy} = 0$) (dashed line) and the mean value of E^* (for $\epsilon_{xx} = \epsilon_{yy} = -0.25\epsilon_{zz}$) (solid line) with strain for the silicon MEAM potential [8] with the z direction aligned with the [111] crystallographic direction.

$C_{13} = 44.21$ GPa, and $C_{55} = 38.3$ GPa and the density is 2.193 g/cm^3, which give $c_R = 3.86$ km/s.

After the full load was applied and the upper and lower surfaces were held fixed in the MD simulations, the crack continued to accelerate for 1–2 ps and then propagated at a constant rate $\pm 10\%$. Crack speeds were determined during the period of steady state propagation, while the crack was in the central region, that is, at least $0.75H$ from either end of the model. Knauss [17] and Rice [18] have shown that the energy release rate is approximately constant in this region. The MD results for normalized crack speed are plotted versus the static energy release rate in Fig. 3. Crack speeds in the $H = 112$ Å model are consistently slightly lower than the two other models, which indicates that H must be larger than 112 Å to avoid boundary effects. The $H = 147$ Å and $H = 239$ Å models give equivalent results. An increase in model dimensions in either the x or y directions produced the same results for crack length versus time within one atomic spacing, in agreement with continuum predictions [17,18].

Experimental results from Hauch *et al.* [1] are also shown in Fig. 3 for comparison. In the MD simulations, cracks did not grow dynamically for $J_s < 3.6$ J/m^2.

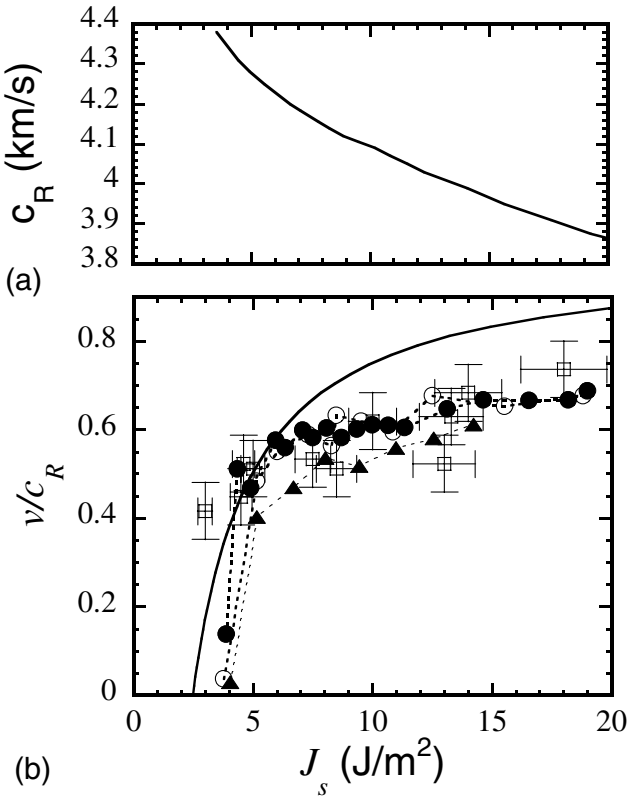

FIG. 3. (a) Variation of Rayleigh wave speed (c_R) with static energy release rate (J_s) in the $H = 147$ Å model. (b) Normalized crack speed (v/c_R) as a function of J_s and model heights $H = 239$ Å (open circle), $H = 147$ Å (full circle), and $H = 112$ Å (full triangle), compared with the experimental results (open square) of Hauch *et al.* [1]. Solid line is continuum prediction for $J_d = 2\gamma_0$.

Experimental results show that $J_{1C} = 2.48$ J/m^2 [9,10]. For $2.5 < J_s < 3.6$ J/m^2, minimization of the energy would cause the crack to grow, but the time scales used in the MD calculations at 300 K (10–30 ps) were not sufficient to observe the initiation of crack growth. These results are can be compared to fracture initiation in simulations by Hauch *et al.* [1] using a modified Stillinger-Weber (SW) potential ($J_{1C} = 5.5$ J/m^2) and by Bernstein and Hess [6] using the tight binding potential ($J_{1C} = 2.1$ J/m^2) and the environmentally dependent interatomic potential (EDIP) ($J_{1C} = 20$ J/m^2).

For $J_s > 3.6$ J/m^2, the crack speed increases rapidly with J_s in the MD simulations, similarly to the experimental results for $J_s > J_{1C}$. For $J_s > 4$ J/m^2, the MD results for the $H = 147$ Å and $H = 239$ Å models agree with the experimental crack speeds within experimental uncertainty. The crack speeds calculated by MD fluctuated by nearly $+10\%$ with variation of the initial conditions. The scatter could be reduced by running the crack for longer times in longer models. In the MD simulations, the crack speed reached a maximum value of $67 \pm 7\%$ of the Rayleigh wave speed compared to the maximum value observed in the experiments: $74 \pm 7\%$ of c_R. The decrease of c_R with increasing J_s for the $H = 147$ Å model is also shown in Fig. 3 for reference. In previous simulations using a modified SW potential [1], the crack speed showed only a slight increase for $J_s > 6$ J/m^2. In simulations using EDIP combined with a tight binding potential [6], crack speed decreased for $J_s > 4$ J/m^2. In those simulations, no variation of c_R was taken into account. The current simulations clearly indicate that a decrease of c_R with J_s is expected, since $H = 150$ Å in [1], and $H = 235$ Å in [6]. The amount of the decrease would depend on the variation of the elastic constants with strain in those potentials. We find that using the normalization v/c_R, correlates models of different height. Much larger models with low strain could be used, in which case no correction for c_R would be necessary. The sizes of models used in this study were chosen for greater efficiency.

In the simulations, fracture always occurred along (111) planes between atoms aligned vertically. For $J_s < 5.5$ J/m^2, fracture resulted in nearly perfect cleavage. For higher values of J_s, dislocations were generated behind the crack tip, resulting in lattice defects as shown in Fig. 4. Since the (111) fracture plane is not a plane of mirror symmetry, differences in the deformation above and below the fracture plane are possible. Dislocations on the upper crack surface were primarily on the (100) plane. On the lower crack surface, dislocations occurred most often on the $(1\overline{1}\overline{1})$ plane, with some dislocations on the (100) plane also. For $J_s > 10$ J/m^2, the crack would occasionally jump from one (111) plane to another located one to five bilayers apart. An example is shown in Fig. 4. The jumps resulted from crack tip blunting, which reduces the tensile stress directly ahead of the crack tip [12]. Crack branching into two or more simultaneously propagating cracks was not observed in these simulations.

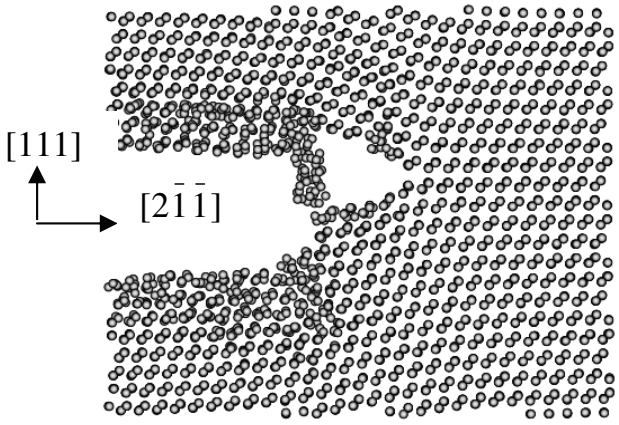

FIG. 4. Detail of a crack propagating in the $H = 147$ Å silicon model for $J_s = 13.1$ J/m^2.

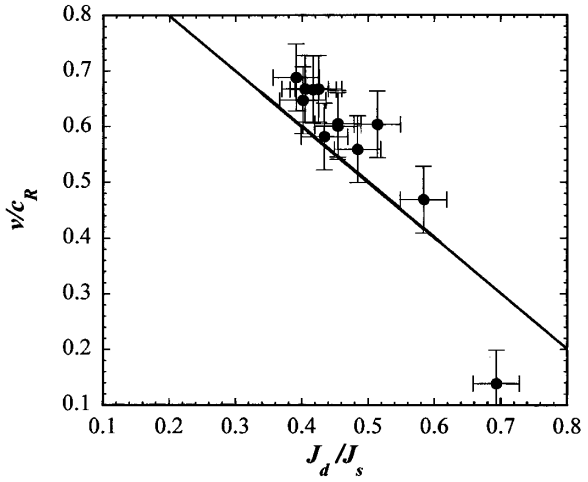

FIG. 5. Normalized crack speed (v/c_R) as a function of J_d/J_s for dynamic fracture in the $H = 147$ Å silicon model. Solid line is the prediction from Eq. (1).

The dislocations and other damage on the crack surfaces resulted in atoms displaced from their lattice positions in the wake of the crack as shown in Fig. 4. The excess energy associated with these displaced atoms and surface atoms was calculated by completely relaxing the $H = 147$ Å model at 0 K after the crack had run completely through it. Then the energy of the atoms in ten bilayers above and below the crack faces was determined for a 100 Å long region where steady crack propagation had occurred. In the absence of any other dissipation mechanism, the energy in excess of the bulk potential energy is equal to the dynamic fracture toughness (J_d). A least squares regression of the data from the $H = 147$ Å model determined that J_d increased linearly with J_s according to: $J_d = 1.15$ J/m^2 + $0.337 J_s$ (regression coefficient, $r = 0.99$). Extrapolation of this linear relation to large values indicates J_d that approaches $(1/3) J_s$. Inserting $J_d = (1/3) J_s$ into Eq. (1) predicts a limiting value of the crack speed equal to $(2/3)c_R$, as observed in the simulations and in agreement with experimental results [1].

In order to test whether Eq. (1) holds for the strip geometry, the results for v/c_R are plotted versus J_d/J_s in Fig. 5. Plotted this way, the prediction from Eq. (1) is a straight line, as shown by the solid line in Fig. 5. The datum point for the lowest crack speed does not agree with the prediction, because the crack has probably not reached steady state. The rest of the data shows approximate agreement with Eq. (1).

The strain energy that is not consumed as J_d is converted into phonon vibrations. Using the modified SW potential, Hauch *et al.* [1] determined that most of the strain energy was converted into phonon vibrations during fracture. Gumbsch *et al.* [19] propose that each bond breaking event leads to phonon vibrations. For a wide range of dynamic fracture toughness, the current results show that the phonon vibration energy is approximately equal to the elastic wave energy predicted by continuum theory for an infinite body.

This research was funded by the U.S. Department of Energy Office of Basic Energy Sciences. The authors would like to acknowledge helpful discussions with R. G. Hoagland and M. Marder. Computer assistance from F. Cherne is also acknowledged.

[1] J. A. Hauch, D. Holland, M. P. Marder, and H. L. Swinney, Phys. Rev. Lett. **82**, 3823 (1999).
[2] T. Cramer, A. Wanner, and P. Gumbsch, Phys. Rev. Lett. **85**, 788 (2000).
[3] D. Holland and M. Marder, Phys. Rev. Lett. **80**, 746 (1998).
[4] D. Holland and M. Marder, Phys. Rev. Lett. **81**, 4029 (1998).
[5] F. F. Abraham, N. Bernstein, J. Q. Broughton, and D. Hess, Mater. Res. Soc. Bull. **25**, 27 (2000).
[6] N. Bernstein and D. Hess, Mater. Res. Soc. Symp. Proc. **653**, 37 (2001).
[7] M. I. Baskes, Phys. Rev. Lett. **59**, 2666 (1987).
[8] M. I. Baskes, Phys. Rev. B **46**, 2727 (1992).
[9] J. J. Gilman, J. Appl. Phys. **31**, 2208 (1960).
[10] R. J. Jacodine, J. Electrochem. Soc. **110**, 524 (1963).
[11] C. P. Chen and M. H. Liepold, Am. Ceram. Soc. Bull. **59**, 469 (1980).
[12] L. B. Freund, J. Mech. Phys. Solids **20**, 129 (1972); J. Appl. Mech. **39**, 1027 (1972); *Dynamic Fracture Mechanics* (Cambridge University Press, Cambridge, United Kingdom, 1990).
[13] J. W. Hutchinson and Z. Suo, Adv. Appl. Mech. **29**, 63 (1992).
[14] S. Nosé, Mol. Phys. **52**, 255 (1984).
[15] W. G. Hoover, Phys. Rev. A **31**, 1695 (1985).
[16] A. N. Darinskii, Wave Motion **25**, 35 (1997).
[17] W. G. Knauss, J. Appl. Mech. **33**, 356 (1966).
[18] J. R. Rice, J. Appl. Mech. **34**, 248 (1967).
[19] P. Gumbsch, S. J. Zhou, and B. L. Holian, Phys. Rev. B **55**, 3445 (1997).